

Approximating constant- Q seismic propagation in the time domain

Tieyuan Zhu^{1*}, José M. Carcione^{2**} and Jerry M. Harris^{1***}

¹Stanford University, Stanford, California, 94305, USA and ²Istituto Nazionale di Oceanografia e di Geofisica Sperimentale (OGS), Borgo Grotta Gigante 42c, 34010 Sgonico, Trieste, Italy

Received October 2012, revision accepted January 2013

ABSTRACT

In this study, we investigate the accuracy of approximating constant- Q wave propagation by series of Zener or standard linear solid (SLS) mechanisms. Modelling in viscoacoustic and viscoelastic media is implemented in the time domain using the finite-difference (FD) method. The accuracy of numerical solutions is evaluated by comparison with the analytical solution in homogeneous media. We found that the FD solutions using three SLS relaxation mechanisms as well as a single SLS mechanism, with properly chosen relaxation times, are quite accurate for both weak and strong attenuation. Although the RMS errors of FD simulations using a single relaxation mechanism increase with increasing offset, especially for strong attenuation ($Q = 20$), the results are still acceptable for practical applications. The synthetic data of the *Marmousi-II* model further illustrate that the single SLS mechanism, to model constant Q , is efficient and sufficiently accurate. Moreover, it benefits from less computational costs in computer time and memory.

Key words: Seismic modelling, Time domain, Standard linear solid, Constant Q

INTRODUCTION

Constant- Q models were developed to approximate seismic attenuation in seismic exploration and seismology, since attenuation is considered to be almost linear with frequency – therefore Q is constant – in many frequency bands (McDonald *et al.* 1958). It is quite reasonable for exploration of seismic data over limited frequency bands. Kjartansson's constant- Q model (Kjartansson 1979) is popular in many seismic applications because it is mathematically simple to implement in the frequency domain, however it is relatively complex in the time domain (Carcione 2007; Carcione 2009). Instead of Kjartansson's constant- Q model, the superposition of several Zener or SLS mechanisms was introduced to approximate constant Q over a specified frequency range in the time domain (Liu, Anderson and Kanamori 1976; Day and Minster 1984;

Carcione, Kosloff and Kosloff 1988a,b,c), which is often called the nearly constant- Q model (Casula and Carcione 1992; Carcione 2007). It has been applied in many 2D and 3D problems such as marine surveys (Hestholm *et al.*, 2006), near-surface environments and reservoirs (Xu and McMechan 1998; Kang and McMechan 1993a,b) and earthquakes (Carcione *et al.*, 2002; Komatitsch *et al.*, 2004; Käser *et al.*, 2007).

A practical problem in superposing SLS mechanisms is how to determine the appropriate number of elements, L , to provide the desired constant- Q behaviour and to save computer costs for solving viscoelastic wave equations, particularly in 3D modelling. The reason is that the introduction of memory variables, proportional to L , involves extra computational costs to solve the equation of motion. In general, $L = 3$ SLS elements is considered to be accurate enough for three-dimensional simulations in geophysical prospecting (Emmerich and Korn, 1987) and global seismology problems (Savage, Komatitsch and Tromp 2010). Blanch, Robertsson and Symes (1995) reported that a single relaxation mechanism yields reasonably accurate results for most practical

*Email: tyzhu@stanford.edu

**Email: jcarcione@inogs.it

***Email: jerry.harris@stanford.edu

applications in seismic exploration but their results are only shown in a relatively narrow range of frequencies.

In this paper, we systematically investigate the accuracy of one and three SLS mechanisms to approximate constant Q over a broad frequency range. We choose a frequency range [5, 125] Hz that usually covers surface seismic applications. The numerical solutions of viscoacoustic and viscoelastic wave equations are obtained with a time-domain FD technique, where relaxation times are conveniently chosen to better approximate the constant- Q model. The accuracy of the results is analysed by comparison with the Green's function analytical solution. Afterwards, we show the comparison of simulating viscoelasticity in complex media with one and three SLS mechanisms.

VISCOELASTIC WAVE MODEL

In linear viscoelasticity, the stress tensor σ is related to the history of the strain tensor ε via a time convolution

$$\sigma = \psi(t) * \partial_t \varepsilon, \quad (1)$$

where $\psi(t)$ is the relaxation function and the symbol '*' denotes time convolution. To obtain the constant- Q model for attenuation that is linear with frequency, we perform a Fourier transform of equation (1)

$$\sigma(\omega) = M(\omega)\varepsilon(\omega), \quad (2)$$

where ω is the angular frequency and $M(\omega)$ is the complex modulus, which is defined as a Fourier transform of the time derivative of the relaxation function $\psi(t)$. Then, the frequency-dependent Q is defined as

$$Q(\omega) = \frac{\text{Re}M(\omega)}{\text{Im}M(\omega)}, \quad (3)$$

where Re and Im take real and imaginary parts, respectively (e.g., Carcione 2007). Although attenuation depends on frequency, it is usually considered to be constant in the exploration frequency bandwidth, e.g., 5–125 Hz. The modulus of the constant- Q model is given by (Kjartansson 1979)

$$M(\omega) = M_r(i\omega/\omega_r)^{\frac{2}{\pi} \arctan \frac{1}{Q}}, \quad (4)$$

where ω_r is a reference frequency and the reference modulus is

$$M_r = \rho c_r^2 \cos^2 \left(\frac{1}{2} \arctan \frac{1}{Q} \right), \quad (5)$$

where ρ and c_r are the mass density and a reference phase velocity (Carcione 2007), respectively. The frequency-dependent

phase velocity is

$$v_p = c_r \left| \frac{\omega}{\omega_0} \right|^{\frac{1}{\pi}} \arctan \frac{1}{Q}, \quad (6)$$

(Carcione 2007).

Let us consider one relaxation mechanism or element (a single Zener element, $L = 1$) and show how its parameters have to be chosen to better approximate the Kjartansson constant- Q model. First, we assume that the reference frequency $\omega_r = \omega_0$ is the central frequency of the source and we force Q of the single peak at that frequency to be Kjartansson's Q , say Q_0 . In the frequency domain, the bulk modulus corresponding to the single peak is

$$M(\omega) = M_R \left(\frac{1 + i\omega\tau_\varepsilon}{1 + i\omega\tau_\sigma} \right), \quad (7)$$

where

$$\tau_\varepsilon = \frac{\tau_0}{Q_0} \left(\sqrt{Q_0^2 + 1} + 1 \right) \quad \text{and} \quad \tau_\sigma = \frac{\tau_0}{Q_0} \left(\sqrt{Q_0^2 + 1} - 1 \right), \quad (8)$$

are relaxation times, with $\tau_0 = \sqrt{\tau_\varepsilon \tau_\sigma} = 1/\omega_0$ and M_R the relaxed modulus given below. To find M_R we force the phase velocity at ω_0 to be the phase velocity of the constant- Q model. Since the phase velocity of the Zener element is

$$v_p = \left[\text{Re} \left(\sqrt{\frac{\rho}{M}} \right) \right]^{-1}, \quad (9)$$

using equation (6) we obtain

$$M_R = \rho c_r^2 \text{Re}^2 \left(\sqrt{\frac{1 + i\omega_0\tau_\sigma}{1 + i\omega_0\tau_\varepsilon}} \right). \quad (10)$$

For L (odd) relaxation mechanisms the theory is given in Carcione (2007), Section 2.4.5. In this case the frequency of the central relaxation peak is ω_0 .

From equations (3) and (7) we obtain Q as a function of frequency.

NUMERICAL EXPERIMENTS

In order to evaluate the accuracy of many SLS mechanisms, we compare numerical solutions with the analytical solution. A 2D analytical solution obtained from the viscoacoustic Green's function in a homogeneous medium is given in Carcione *et al.* (1988a).

We perform two tests with $Q = 100$ and $Q = 20$, which are typical Q values for sedimentary rocks. The tested model is a homogeneous medium with velocity 3.5 km/s and density 2.4 g/cm³. The centre frequency of the Ricker-wavelet source

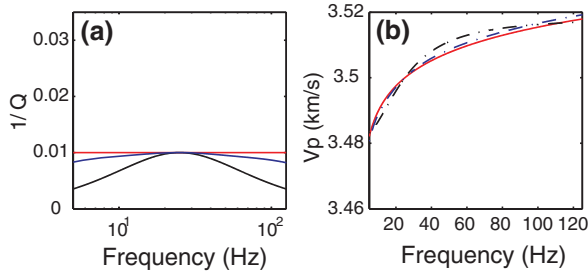


Figure 1 Red (constant $Q = 100$), blue (three SLS, $Q_0 = 58$) and black (one SLS, $Q_0 = 100$) lines representing the dissipation factor (a) and phase velocity (b).

is 25 Hz and the frequency band is 5–125 Hz. For three SLS mechanisms, $\tau_0 = 1/\omega_0$ is determined in an equally spaced logarithmic frequency range. We consider three source-receivers distances: 500 m, 2500 m and 4500 m, the latter of which is a very extreme case for $Q = 20$.

In the first example Q is 100. The dissipation factor ($1/Q$) and phase velocity of three and one SLS mechanisms are shown in Fig. 1. It is not surprising that the three SLS fits the theoretical model curves very well in the specified frequency

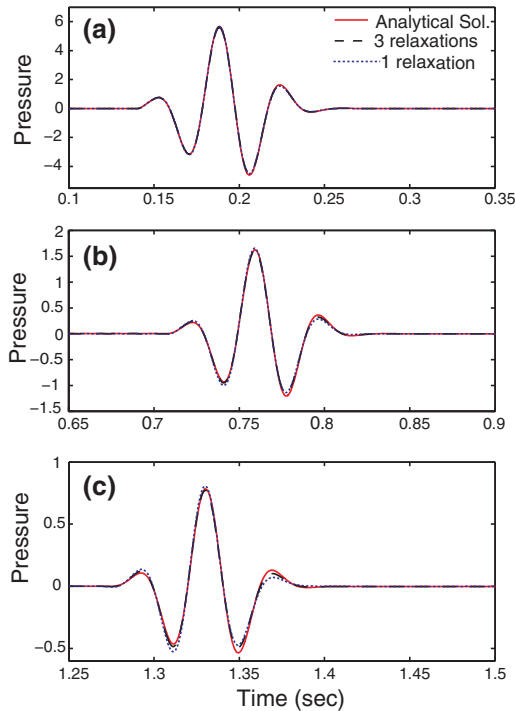


Figure 2 Comparison between the FD and analytical solutions where the source-receiver distances are (a) 500 m, (b) 2500 m and (c) 4500 m. Q is 100.

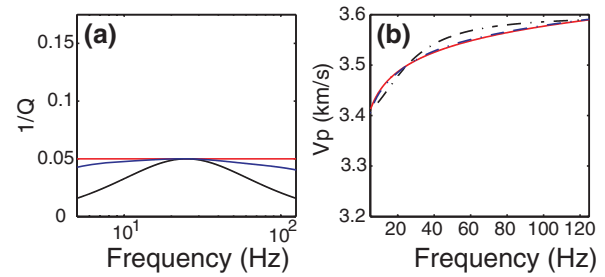


Figure 3 Red (constant $Q = 20$), blue (three SLS, $Q_0 = 12$) and black (one SLS, $Q_0 = 20$) lines representing the dissipation factor (a) and phase velocity (b).

band. Interestingly, the single SLS has a good approximation to the phase velocity and dissipation factor around the reference frequency.

In Fig. 2 we compare the FD results with the analytical Q solution using the constant- Q model. The numerical and analytical solutions agree very well (Fig. 2a). At far offsets (Fig. 2b), we can see that the single SLS mechanism also yields comparable results.

The accuracy is further assessed by using the RMS error, which is defined as

$$E = \frac{\sum_{j=1}^{nt} (d_j^n - d_j^a)^2}{\sum_{j=1}^{nt} (d_j^a)^2} \quad (11)$$

Where nt is the number of time samples of the seismic trace, d_j^n is the calculated value of the numerically simulated trace at sample j and the superscript a is the corresponding analytical value. The RMS errors are listed in Table 1. We can verify that these errors are quite small and that the single SLS mechanism is a good approximation to constant Q .

In the strong attenuation case, i.e., constant $Q = 20$, the dissipation factor and phase velocity of the three and one SLS mechanisms are shown in Fig. 3. Again, the three SLS approximates fairly well to the theoretical model in the specified frequency band while the single SLS has a good approximation

Table 1 Comparison of RMS errors of two relaxation mechanisms for $Q = 100$.

Error with offset	L = 1	L = 3
500 m	2.62e-4	3.94e-4
2500 m	0.0038	0.0014
4500 m	0.0122	0.0040

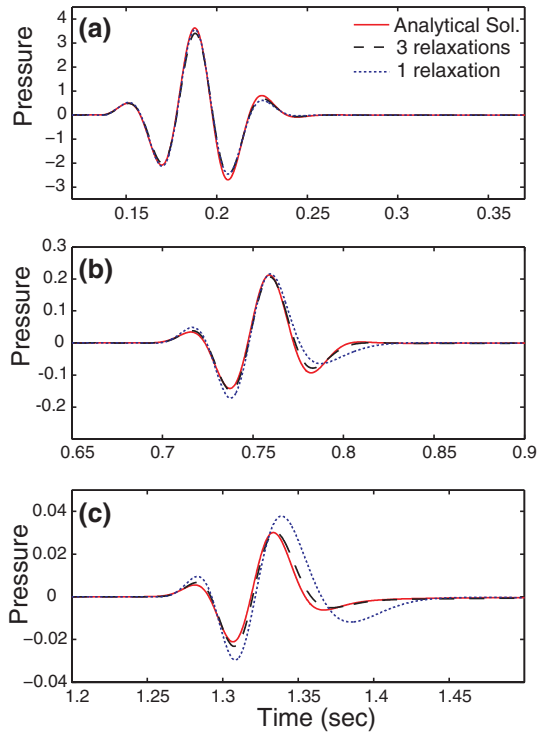


Figure 4 Comparison between the FD and analytical solutions where the source-receiver distances are (a) 500 m, (b) 2500 m and (c) 4500 m. Q is 20.

Table 2 Comparison of RMS errors of two relaxation mechanisms for $Q = 20$.

Error with offset	$L = 1$	$L = 3$
500 m	0.0052	0.0068
2500 m	0.0835	0.0108
4500 m	0.6307	0.0706

to the phase velocity and dissipation factor around the reference frequency.

In Fig. 4 we show comparisons between the FD results and the analytical solution. The numerical and analytical solutions also agree very well (Fig. 4a). At far offsets (Fig. 4b,c), the single SLS mechanism is not so accurate (see RMS errors in Table 2). Nevertheless, we note that the amplitude at 4500 m offset is approximately one hundred times smaller than that at 500 m. In exploration geophysics or earthquake seismology, it is improbable to find a situation where a wave propagates such long distances in media with such a low Q value. In addition, at these distances noise would dominant the signal. Hence, we consider that a single SLS, with the parameters chosen as

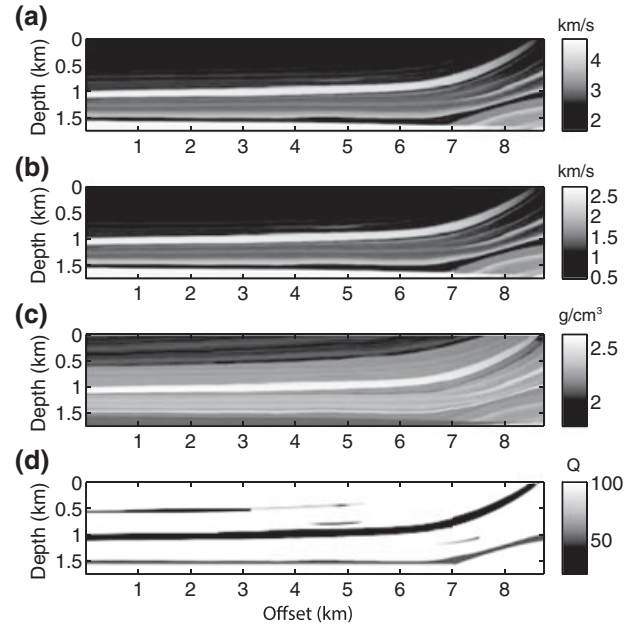


Figure 5 Synthetic models: (a) P-wave velocity; (b) S-wave velocity; (c) density; (d) Q model.

indicated above, approximates sufficiently well a constant- Q medium. Moreover, in view of the realistic simulations that we shall perform below, we also consider the case $L = 3$.

Synthetic model

To further evaluate the accuracy of the SLS mechanisms we consider the *Marmousi-II* elastic model (Martin, Wiley and Marfurt 2006), which is a representative model including continuous and discontinuous parameter changes. We cut the left corner of the *Marmousi-II* elastic model for simulation to reduce computational costs and help analyse and easily identify types of waves in the wavefield for comparison. Figure 5 shows the elastic properties – P-wave velocity, S-wave velocity and density. The attenuation ($1/Q$) properties are based on lithology information. For example, we take $Q = 50$ for the water-saturated sand, $Q = 35$ for the oil-saturated sand and $Q = 20$ for the gas-saturated sand, while the background rock has $Q = 100$ (Fig. 5d).

Viscoacoustic case

The first-order pressure-velocity viscoacoustic wave equation is used to compute the synthetic seismograms (see details in the Appendix). The staggered-grid FD solver has 2nd-order accuracy in time and 4th-order accuracy in space. To minimize

numerical dispersion, ten samples per wavelength are required for the lowest velocity in the model (Robertsson, Blanch and Symes 1994). The model has 471×1870 grid points and we use a time step $dt = 0.25$ ms. The grid spacing in the x and z directions is 5 m. A pressure source is located at $(z_s, x_s) = (250 \text{ m}, 4300 \text{ m})$, which is a zero-phase Ricker wavelet with a centre frequency of 25 Hz. To reduce artificial reflections that are introduced by the edge of the computational grid, an absorbing boundary condition (Cerjan, Kosloff and Reshef 1985) is applied to the sides and bottom of the model.

Figure 6 shows the FD synthetic data – acoustic and viscoacoustic with two scenarios ($L = 3$ and $L = 1$). The same colour scale was applied for comparison. As expected, major features, including first arrivals, refractions, reflections, diffractions and multiples are evident in both the acoustic and viscoacoustic simulated data. However, the viscoacoustic signals are weaker, particularly the multiples. The strong reflections are also reduced in amplitude and have a small phase delay due to velocity dispersion.

The difference waveforms between the acoustic and viscoacoustic data are illustrated in Fig. 7. Two viscoacoustic data are quite close together since the total energy (definition: $\sum \text{diff}^2$) in Fig. 7(b) is about 1.5% of that in Fig. 7(a). Figure 8 shows trace number 200 for the three cases of Fig. 6. As we can verify, the viscoacoustic solutions are very close together. However, the CPU times (2.93 GHz Intel Core 2 Duo) for the single and three SLS relaxation mechanism schemes are 5.3 and 7.8 min, respectively. It is evident that the FD

simulation with the single relaxation mechanism requires less computational effort (see Table 3). Moreover, the number of first-order equations to solve for the viscoacoustic wave equation is $3+L$ in 2D space and $4+L$ in 3D space. These results illustrate that the viscoacoustic simulation with a single SLS mechanism can accurately and efficiently capture attenuation described by the constant- Q model.

Viscoelastic case

To be realistic, we extend the investigation of the accuracy of SLS mechanisms to describe the constant- Q model in viscoelastic media. The first-order pressure-velocity viscoelastic wave equation (see the Appendix) is solved by the staggered-grid finite-difference method with 2nd-order temporal accuracy and 4th-order spatial accuracy. In the elastic model, the minimum velocity is approximately 500 m/s. The grid spacing of 1.25 m in the x and z directions is chosen on the basis of numerical dispersion criteria (Robertsson *et al.* 1994). The same 2D model is discretized with 1521×7120 grid points and we use a time step $dt = 0.15$ ms. A pressure source is located at $(z_s, x_s) = (246.25 \text{ m}, 4301.25 \text{ m})$, which is a zero-phase Ricker wavelet with a centre frequency of 25 Hz.

Figure 9 shows the elastic and viscoelastic FD synthetic data corresponding to the x and z components. We observe the attenuation effects in the reduced amplitude and delayed traveltimes. To evidence the difference between the $L = 3$ and $L = 1$ viscoelastic data – Fig. 9(c) and Fig. 9(e), Fig. 9(d)

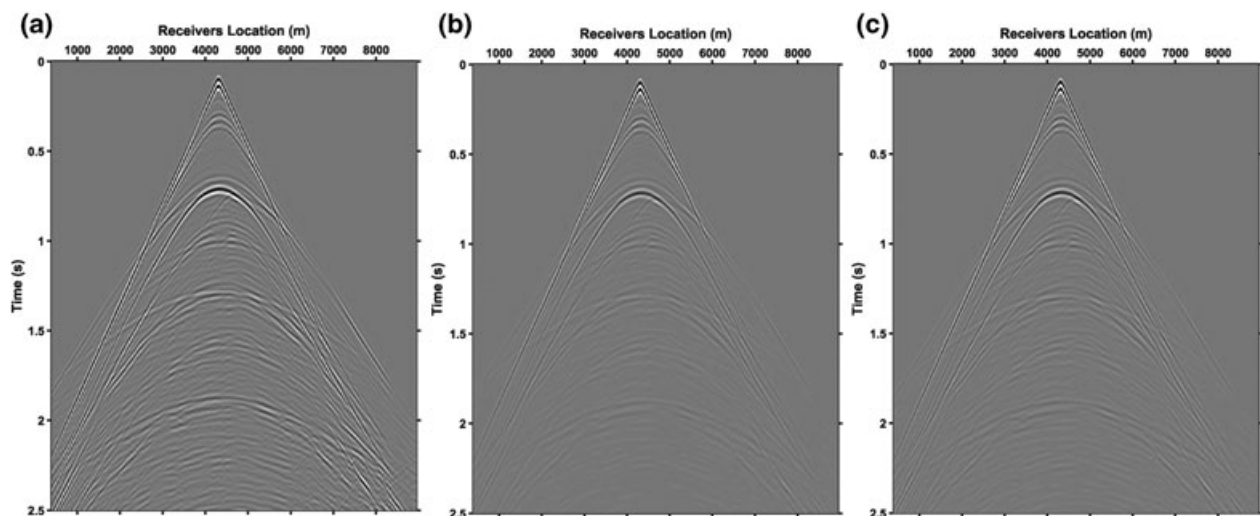


Figure 6 FD synthetic data. (a) Acoustic; (b) viscoacoustic ($L = 3$); (c) viscoacoustic ($L = 1$).

and Fig. 9(f), we subtract the data and examine the difference waveforms illustrated in Fig. 10. Apparently, the difference between the two viscoelastic cases is quite small and the total energy in Fig. 10(c,d) is about 2% of that in Fig. 10(a,b) (difference between the elastic and viscoelastic seismograms). Trace number 200 of the three cases is illustrated in Fig. 11 that confirms this observation. From a computational point of view, the FD simulation with a single SLS mechanism is more than two times faster than that with three SLS mechanisms (see Table 3). In this case, the number of first-order equations to solve is $5 + 3L$ in 2D space and $9 + 6L$ in 3D space (see the Appendix). The number of equations to solve in the single SLS mechanism case is nearly 45% less than those of the three SLS mechanisms. It can be concluded that one may safely use the one single SLS mechanism to describe the constant- Q model, which requires less computational time and storage than that of the three SLS mechanisms.

CONCLUSIONS

We have investigated the accuracy of the Zener or standard linear solid model (SLS) to approximate constant Q in the time domain. The comparison of numerical FD results against analytical solutions clearly shows a similar accuracy between one SLS element and three SLS mechanisms. We showed that FD simulations using a single SLS mechanism are sufficiently accurate and efficient for most practical applications.

Table 3 Computational costs of the Marmousi-II model.

	Lossless	$L = 3$	$L = 1$
Acoustic	3.6 min	7.8 min	5.3 min
Viscoelastic	1.4 hr	15 hr	7.3 hr

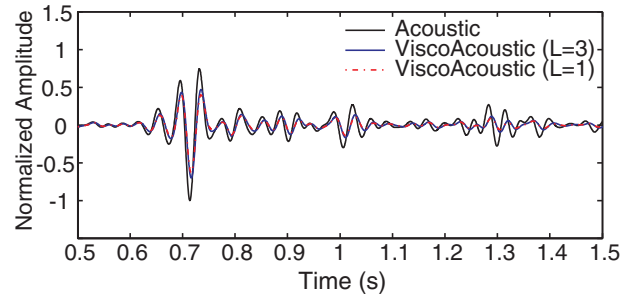


Figure 8 Comparison of trace number 200 of acoustic (black), $L = 3$ viscoacoustic (blue) and $L = 1$ viscoacoustic (red).

We have considered the viscoacoustic and viscoelastic wave equations. In the viscoacoustic case, modelling constant Q with a single SLS mechanism is faster than using three SLS mechanisms, because four memory-variable equations have to be solved instead of six.

In the viscoelastic case, the use of a single SLS mechanism is much more convenient. Modelling constant Q with a single SLS mechanism is more than two times faster than using three

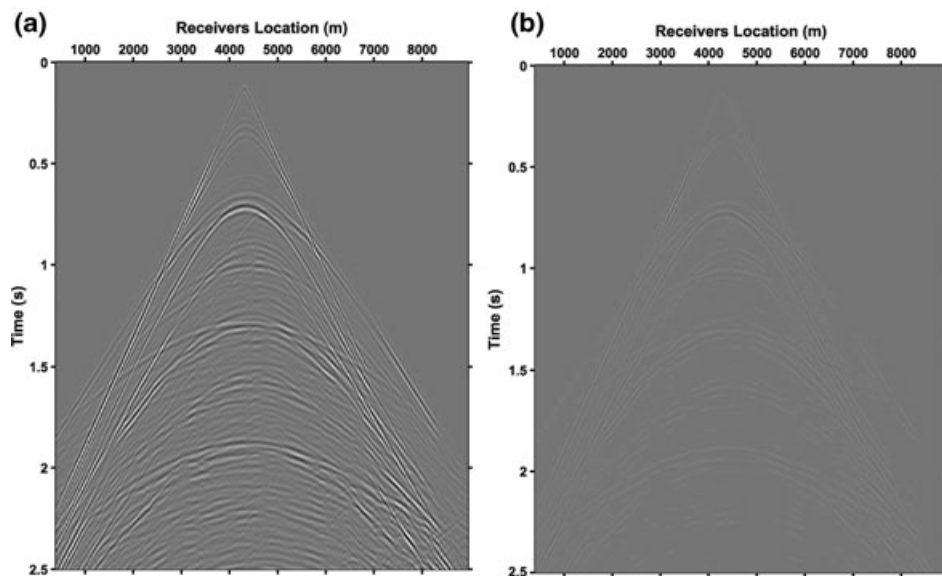


Figure 7 (a) Difference between acoustic and viscoacoustic ($L = 3$). (b) Difference between viscoacoustic ($L = 3$) and viscoacoustic ($L = 1$).

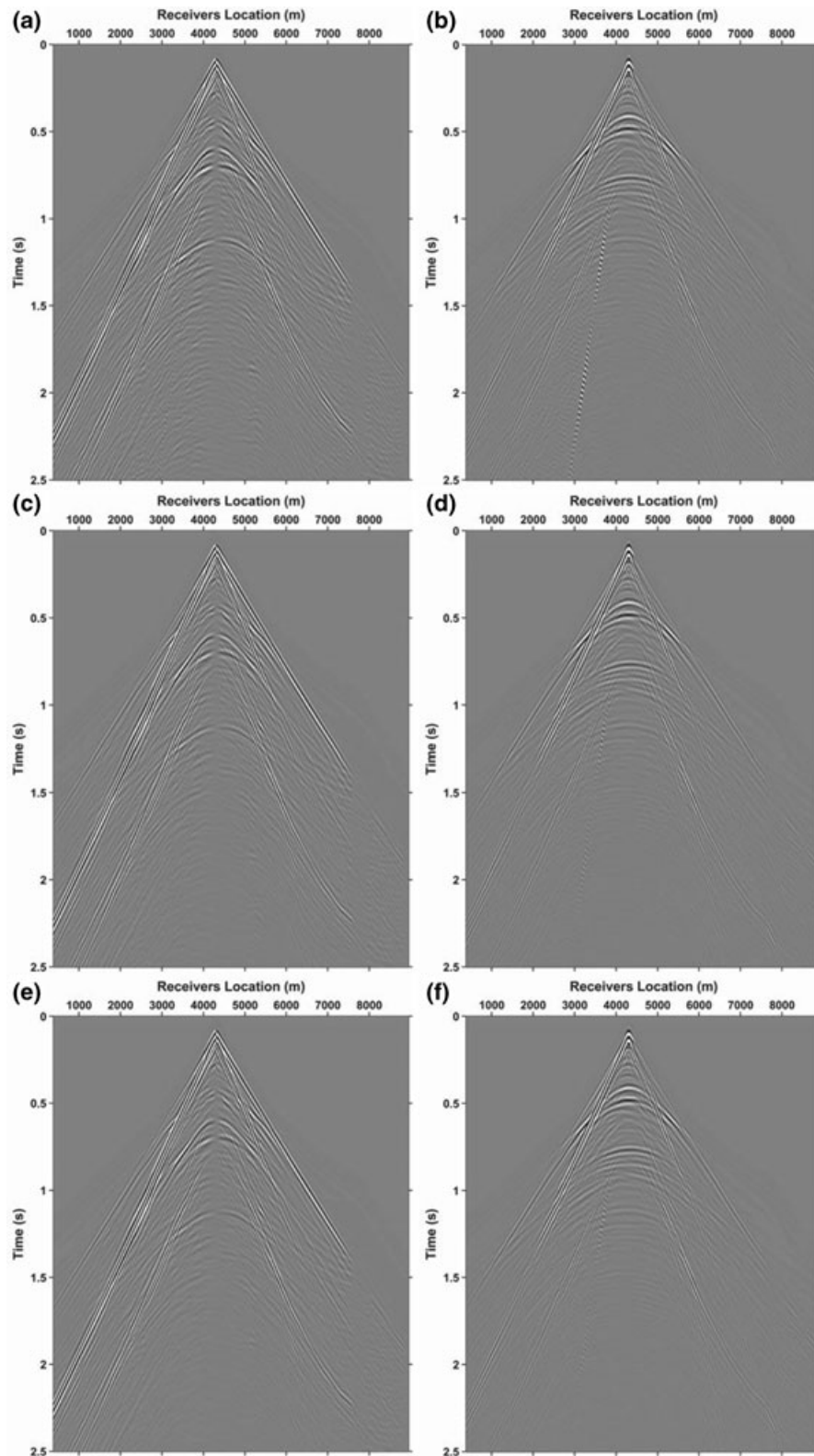


Figure 9 Elastic data, (a) x -component, (b) z -component; $L = 3$ viscoelastic data in the x -component (c) and z -component (d); $L = 1$ viscoelastic data in the x -component (e) and z -component (f).

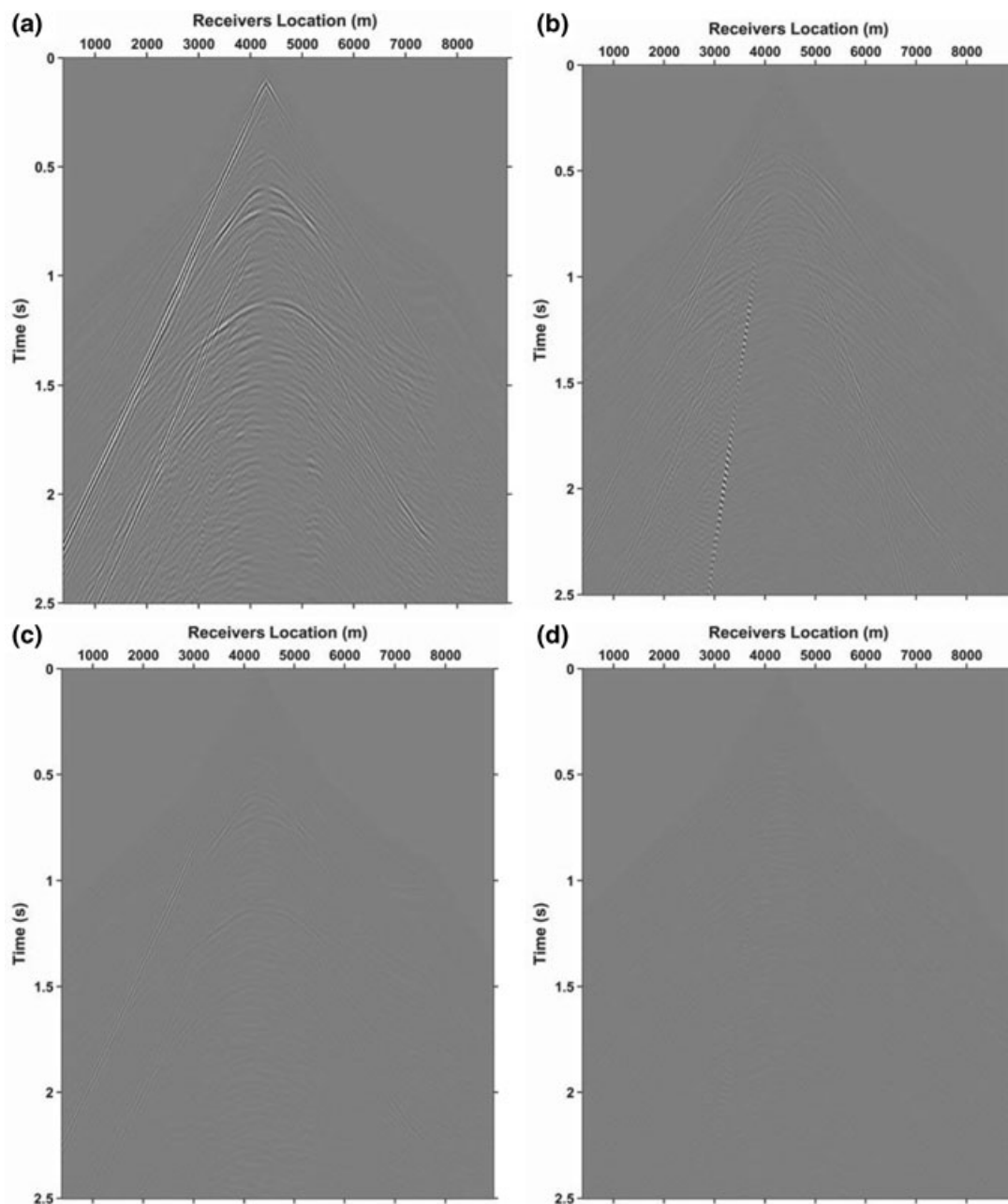


Figure 10 (a) Difference between elastic (Fig. 9a) and viscoelastic (Fig. 9c) x -component data; (b) difference between elastic (Fig. 9b) and viscoelastic (Fig. 9d) z -component data; (c) difference between viscoelastic (Fig. 9c) and viscoelastic (Fig. 9e) x -component data; (d) difference between viscoelastic (Fig. 9d) and viscoelastic (Fig. 9f) z -component data;

SLS mechanisms, because eight memory-variable equations have to be solved instead of fourteen. Moreover, in 3D space the saving in computer time and storage will be substantial. In this case it is advisable to use high-order finite difference methods or alternatively the Fourier pseudospectral method that

uses two grid points per minimum wavelength. This work also shows that fitting a constant Q model can be avoided and use of a single mechanism with properly chosen parameters is sufficient. Therefore, we suggest that a single SLS mechanism is an efficient approach to model constant Q for computational

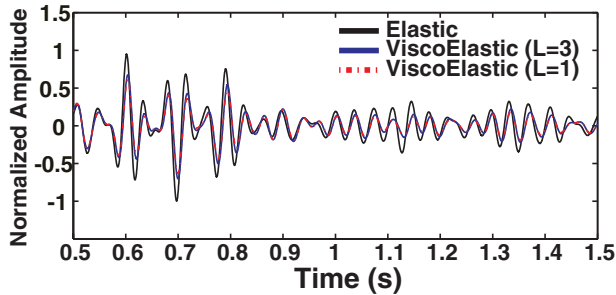


Figure 11 Comparison of trace number 200 of elastic (black), $L = 3$ viscoelastic (blue) and $L = 1$ viscoelastic (red).

intensive seismic modelling and inversion in practical applications.

ACKNOWLEDGEMENTS

We would like to thank editor Felix Herrmann and anonymous reviewers for their valuable comments. T. Zhu would like to thank Stanford Wave Physics Laboratory for financial support and Xiaobi Xie for discussions of the Green's function analytical solution. J.M. Carcione thanks the EU-CO2CARE project for partially funding his research.

REFERENCES

- Blanch J.O., Robertsson J.O. and Symes W.W. 1995. Modeling of a constant Q : Methodology and algorithm for an efficient and optimally inexpensive viscoelastic technique. *Geophysics* **60**, 176–184.
- Carcione J.M. 2007. Wavefields in Real Media. *Theory and Numerical Simulation of Wave Propagation in Anisotropic, Anelastic, Porous and Electromagnetic Media*. Elsevier Science.
- Carcione J.M. 2009. Theory and modeling of constant- Q P- and S-waves using fractional time derivatives. *Geophysics* **74**, T1–T11.
- Carcione J.M., Helle H.B., Seriani G. and Plasencia Linares M.P. 2002. Simulation of seismograms in a 2-D viscoelastic Earth by pseudospectral methods. *Geofísica Internacional* **44**(2), 123–142.
- Carcione J.M., Kosloff D. and Kosloff R. 1988a. Wave propagation in a linear viscoacoustic medium. *Geophysical Journal of the Royal Astronomical Society* **93**, 393–407.
- Carcione J. M., Kosloff D. and Kosloff R. 1988b. Viscoacoustic wave propagation simulation in the Earth. *Geophysics* **53**, 769–777.
- Carcione J.M., Kosloff D. and Kosloff R. 1988c. Wave propagation in a linear viscoelastic medium. *Geophysical Journal of the Royal Astronomical Society* **95**, 597–611.
- Casula G. and Carcione J.M. 1992. Generalized mechanical model analogies of linear viscoelastic behaviour. *Bollettino di Geofisica Teorica ed Applicata* **34**, 235–256.
- Cerjan C., Kosloff D. and Reshef M. 1985. A non-reflecting boundary condition for discrete acoustic and elastic wave equation. *Geophysics* **50**, 705–708.

- Day S.M. and Minster J.B. 1984. Numerical simulation of attenuated wavefield using a Padé approximant method. *Geophysical Journal of the Royal Astronomical Society* **78**, 105–118.
- Emmerich H. and Korn M. 1987. Incorporation of attenuation into time-domain computations of seismic wavefields. *Geophysics* **52**, 1252–1264.
- Kang I.B. and McMechan G.A. 1993a. Effects of visco-elasticity on seismic wave propagation in fault zones, near surface sediments, and inclusions. *Bulletin of the Seismological Society of America* **83**, 890–906.
- Kang I.B. and McMechan G.A. 1993b. Visco-elastic seismic responses of 2-D reservoir models. *Geophysical Prospecting* **41**, 149–163.
- Käser M., Dumbser M., de la Puente J. and Igel H. 2007. An arbitrary high-order discontinuous Galerkin method for elastic waves on unstructured meshes – III. Viscoelastic attenuation. *Geophysical Journal International* **168**, 224–242.
- Kjartansson E. 1979. Constant- Q wave propagation and attenuation. *Journal of Geophysical Research* **84**, 4737–4748.
- Komatitsch D., Liu Q., Tromp J., Suss P., Stidham C. and Shaw J. H. 2004. Simulations of ground motion in the Los Angeles basin based upon the spectral-element method. *Bulletin of the Seismological Society of America* **94**(1), 187–206.
- Hestholm S., Ketcham S., Greenfield R., Moran M. and McMechan G.A. 2006. Quick and accurate Q -parameterization in viscoelastic wave modeling. *Geophysics* **71**, T147–T150.
- Liu H.P., Anderson D.L. and Kanamori H. 1976. Velocity dispersion due to anelasticity: Implication for seismology and mantle composition. *Geophysical Journal of the Royal Astronomical Society* **47**, 41–58.
- Martin G. S., Wiley R. and Marfurt K. J. 2006. Marmousi – 2: An elastic upgrade for Marmousi. *The Leading Edge* **25**, 156–166.
- McDonal F.J., Angona F.A., Mills R.L., Sengbush R.L., Van Nostrand R.G. and White J.E. 1958. Attenuation of shear and compressional waves in Pierre shale. *Geophysics* **23**, 421–439.
- Robertsson J.O., Blanch J.O. and Symes W.W. 1994. Viscoelastic finite-difference modeling. *Geophysics* **59**, 1444–1456. doi:10.1190/1.1443701
- Savage B., Komatitsch D. and Tromp J. 2010. Effects of 3D attenuation on seismic wave amplitude and phase measurements. *Bulletin of the Seismological Society of America* **100**(3), 1241–1251.
- Xu T. and McMechan G.A. 1998. Efficient 3-D viscoelastic modeling with application to near-surface data. *Geophysics* **63**, 601–612.

APPENDIX

Viscoacoustic and viscoelastic wave equations

The complete time-domain equations for wave propagation in heterogeneous viscoacoustic and viscoelastic media can also be found in Carcione (2007).

Viscoacoustic wave equation

Assuming pressure $P = -\sigma_{ii}$ ($i = x, y, z$) is viscoacoustic and σ is the stress, the viscoacoustic P-SV velocity/stress equations in 3D are written below.

1) Euler-Newton's equations

$$\begin{aligned}\rho \frac{\partial v_x}{\partial t} &= -\frac{\partial P}{\partial x} + f_x, \\ \rho \frac{\partial v_y}{\partial t} &= -\frac{\partial P}{\partial y} + f_y, \\ \rho \frac{\partial v_z}{\partial t} &= -\frac{\partial P}{\partial z} + f_z,\end{aligned}\quad (\text{A1})$$

where v_x , v_y and v_z are the particle velocities, ρ is the bulk density and f_x , f_y and f_z are the body forces.

2) Stress-strain relations:

$$\frac{\partial P}{\partial t} = -M_R M_l \left(\frac{\partial v_x}{\partial x} + \frac{\partial v_y}{\partial y} + \frac{\partial v_z}{\partial z} \right) - \frac{M_R}{L} \sum_{l=1}^L r_l, \quad (\text{A2})$$

3) Memory variable equations:

$$\frac{\partial r_l}{\partial t} = \frac{1}{\tau_{\sigma l}} \left[\left(1 - \frac{\tau_{\epsilon l}}{\tau_{\sigma l}} \right) \left(\frac{\partial v_x}{\partial x} + \frac{\partial v_y}{\partial y} + \frac{\partial v_z}{\partial z} \right) - r_l \right], \quad (\text{A3})$$

where r is the first time derivative of the memory variable ($\partial e/\partial t$) (Carcione 2007, page 95). M_R is the relaxed Lamé constant. The complex Zener modulus is written as:

$$M_l = 1 - \frac{1}{L} \sum_{l=1}^L \left(1 - \frac{\tau_{\epsilon l}}{\tau_{\sigma l}} \right) = 1 - \frac{1}{L} \sum_{l=1}^L \frac{\tau_{\epsilon l}}{\tau_{\sigma l}}, \quad (\text{A4})$$

where L is the number of mechanisms. The relaxation times can be expressed as

$$\tau_{\sigma l} = \frac{\tau_0}{Q_{0l}} \left(\sqrt{1 + Q_{0l}^2} - 1 \right), \quad \tau_{\epsilon l} = \frac{\tau_0}{Q_{0l}} \left(\sqrt{1 + Q_{0l}^2} + 1 \right), \quad (\text{A5})$$

where $\tau_0 = \frac{1}{\omega_0}$, ω_0 is the centre angular frequency of the relaxation peak. Q_{0l} are the minimum quality factors. $\tau_{\epsilon l}$ is equal to $\tau_{\sigma l}$ in the elastic case.

Viscoelastic wave equation

The viscoelastic P-SV velocity/stress equations in 3D space are formulated in equations (A6)–(A9).

1) Euler-Newton's equation:

$$\begin{aligned}\rho \frac{\partial v_x}{\partial t} &= -\left(\frac{\partial \sigma_{xx}}{\partial x} + \frac{\partial \sigma_{xy}}{\partial y} + \frac{\partial \sigma_{xz}}{\partial z} \right) + f_x, \\ \rho \frac{\partial v_y}{\partial t} &= -\left(\frac{\partial \sigma_{xy}}{\partial x} + \frac{\partial \sigma_{yy}}{\partial y} + \frac{\partial \sigma_{yz}}{\partial z} \right) + f_y, \\ \rho \frac{\partial v_z}{\partial t} &= -\left(\frac{\partial \sigma_{xz}}{\partial x} + \frac{\partial \sigma_{yz}}{\partial y} + \frac{\partial \sigma_{zz}}{\partial z} \right) + f_z,\end{aligned}\quad (\text{A6})$$

2) Stress-strain relations:

$$\begin{aligned}\frac{\partial \sigma_{xx}}{\partial t} &= (\lambda_u + 2\mu_u) \frac{\partial v_x}{\partial x} + \lambda_u \left(\frac{\partial v_y}{\partial y} + \frac{\partial v_z}{\partial z} \right) \\ &\quad + \left(\lambda_r + \frac{2}{n} \mu_r \right) \sum_{l=1}^{L_1} r_{1l} + 2\mu_r \sum_{l=1}^{L_2} r_{11l}, \\ \frac{\partial \sigma_{yy}}{\partial t} &= (\lambda_u + 2\mu_u) \frac{\partial v_y}{\partial y} + \lambda_u \left(\frac{\partial v_x}{\partial x} + \frac{\partial v_z}{\partial z} \right) \\ &\quad + \left(\lambda_r + \frac{2}{n} \mu_r \right) \sum_{l=1}^{L_1} r_{1l} + 2\mu_r \sum_{l=1}^{L_2} r_{22l}, \\ \frac{\partial \sigma_{zz}}{\partial t} &= (\lambda_u + 2\mu_u) \frac{\partial v_z}{\partial z} + \lambda_u \left(\frac{\partial v_x}{\partial x} + \frac{\partial v_y}{\partial y} \right) \\ &\quad + \left(\lambda_r + \frac{2}{n} \mu_r \right) \sum_{l=1}^{L_1} r_{1l} - 2\mu_r \sum_{l=1}^{L_2} (r_{11l} + r_{22l}), \\ \frac{\partial \sigma_{xy}}{\partial t} &= \mu_u \left(\frac{\partial v_x}{\partial y} + \frac{\partial v_y}{\partial x} \right) + \mu_r \sum_{l=1}^{L_2} r_{12l}, \\ \frac{\partial \sigma_{xz}}{\partial t} &= \mu_u \left(\frac{\partial v_x}{\partial z} + \frac{\partial v_z}{\partial x} \right) + \mu_r \sum_{l=1}^{L_2} r_{13l}, \\ \frac{\partial \sigma_{yz}}{\partial t} &= \mu_u \left(\frac{\partial v_y}{\partial z} + \frac{\partial v_z}{\partial y} \right) + \mu_r \sum_{l=1}^{L_2} r_{23l},\end{aligned}\quad (\text{A7})$$

where $\lambda_u = (\lambda_r + \frac{2}{n} \mu_r) M_{U1} - \frac{2}{n} \mu_r M_{U2}$, $\mu_u = \mu_r M_{U2}$. For the general standard linear solid rheology, they are given by $M_{Uv} = 1 - \frac{1}{L_v} \sum_{l=1}^{L_v} \left(1 - \frac{\tau_{\epsilon l}^{(v)}}{\tau_{\sigma l}^{(v)}} \right)$, $v = 1, 2$.

Two relaxation mechanisms are used $v = 1, 2$ – they are the dilatational and shear modes.

3) Memory-variable equations:

$$\begin{aligned}\frac{\partial r_{1l}}{\partial t} &= \phi_{1l} \theta - \frac{r_{1l}}{\tau_{\sigma l}^{(1)}}, \\ \frac{\partial r_{11l}}{\partial t} &= \phi_{2l} \left(\frac{\partial v_x}{\partial x} - \frac{\theta}{n} \right) - \frac{r_{11l}}{\tau_{\sigma l}^{(2)}}, \\ \frac{\partial r_{22l}}{\partial t} &= \phi_{2l} \left(\frac{\partial v_y}{\partial y} - \frac{\theta}{n} \right) - \frac{r_{22l}}{\tau_{\sigma l}^{(2)}}, \\ \frac{\partial r_{12l}}{\partial t} &= \phi_{2l} \left(\frac{\partial v_x}{\partial y} + \frac{\partial v_y}{\partial x} \right) - \frac{r_{12l}}{\tau_{\sigma l}^{(2)}}, \\ \frac{\partial r_{13l}}{\partial t} &= \phi_{2l} \left(\frac{\partial v_x}{\partial z} + \frac{\partial v_z}{\partial x} \right) - \frac{r_{13l}}{\tau_{\sigma l}^{(2)}}, \\ \frac{\partial r_{23l}}{\partial t} &= \phi_{2l} \left(\frac{\partial v_y}{\partial z} + \frac{\partial v_z}{\partial y} \right) - \frac{r_{23l}}{\tau_{\sigma l}^{(2)}},\end{aligned}\quad (\text{A8})$$

where

$$\begin{aligned}\phi_{vl} &= \frac{1}{\tau_{\sigma l}^{(v)}} \left(1 - \frac{\tau_{\epsilon l}^{(v)}}{\tau_{\sigma l}^{(v)}} \right) \frac{\partial r_l}{\partial t} \\ \theta &= \frac{\partial v_x}{\partial x} + \frac{\partial v_y}{\partial y} + \frac{\partial v_z}{\partial z},\end{aligned}\quad (\text{A9})$$

where r is the first time derivative of the memory variable ($\partial e/\partial t$).